Available online at website: https://journal.bcrec.id/index.php/bcrec

Bulletin of Chemical Reaction Engineering & Catalysis, 20 (4) 2025, 594-606

Original Research Article

Photocatalytic Degradation of Methyl Orange Using TiO_2 - Coated Cordierite Substrates: A Comparison of Dip-Coating and Spray-Coating Methods

Trung Hieu Nguyen[1], Thu Huong Nguyen[2], Anh-Tuan Vu[2], Thang Le Minh[2,*]

[1]School of Materials Science and Engineering, Hanoi University of Science and Technology, Hanoi, Vietnam
[2]School of Chemistry and Life Sciences, Hanoi University of Science and Technology, Hanoi, Vietnam.

Received: 20th May 2025; Revised: 3rd September 2025; Accepted: 6th September 2025
Available online: 11th September 2025; Published regularly: December 2025

Abstract

In this study, the calcination temperature of TiO_2 nanoparticles was investigated at 300, 350, 400, and 450 °C. The results indicated that 400 °C was the optimal calcination temperature, yielding the highest amount of synthesized TiO_2 nanoparticles remaining in the anatase phase (97.44 %). TiO_2 nanoparticles were coated on cordierite using two methods: spray coating and dip coating. Their characteristics were analyzed and evaluated utilizing several modern techniques. Additionally, their photocatalytic and recovery capabilities were assessed based on methylene orange (MO) degradation efficiency. The spray coating method allowed the TiO_2 nanoparticles to evenly cover the cordierite surface, resulting in the highest MO degradation efficiency and best recovery ability. The MO degradation efficiency remained at 83.07 % after 5 reuse cycles.

Keywords: Titanium oxide; Methyl Orange; Photocatalytic; Coating

How to Cite: Nguyen, T.H., Nguyen, T.H., Vu, A.-T., Minh, T.L. (2025). Photocatalytic Degradation of Methyl Orange Using TiO2 - Coated Cordierite Substrates: A Comparison of Dip-Coating and Spray-Coating Methods. *Bulletin of Chemical Reaction Engineering & Catalysis*, 20 (4), 594-606. (doi: 10.9767/bcrec.20400)

Permalink/DOI: https://doi.org/10.9767/bcrec.20400

1. Introduction

The water pollution problem is increasingly alarming in the world [1,2]. There are many sources cause water pollution. Among them, industrial waste and domestic waste are two sources of waste containing the most toxic pollutants including antibiotics, persistent organic substances, and heavy metals, etc [3-6]. This problem causes many negative impacts on the ecosystem and human health [7,8]. Worldwide, about 14,000 people die every day as a result of water pollution. Dye pollution in industrial wastewater, particularly from the textile, footwear, and paper industries, is becoming a significant environmental concern. Synthetic dyes often have a stable structure, are difficult to biodegrade, leading to long-term persistence in the aquatic environment. When entering the body, they can cause many harmful effects on human health, such as liver and kidney dysfunction, immune deficiency, and even potential cancer risk [9]. In addition, dyes also hinder the photosynthesis process of aquatic organisms by reducing light transmission, causing ecosystem imbalance, biodiversity loss, and food chain pollution. This is a major challenge that requires effective treatment solutions to protect public health and the environment. Therefore, solutions need to be researched to address this problem. Some of the methods used today to resolve this problem include adsorption, photocatalysis, biodegradation, and electrolysis, etc. [10-14]. Advanced Oxidation Processes

* Corresponding Author.
Email: thang.leminh@hust.edu.vn (T.L. Minh);
hieu.nguyentrung@hust.edu.vn (T.H. Nguyen)

(AOPs) are one of the effective techniques used to treat and degrade dyes in wastewater [15]. The main mechanism of this method is based on the creation of hydroxyl radicals (•OH) with strong oxidizing properties, capable of attacking and breaking down the stable aromatic ring structure of dye molecules. Common AOPs processes include ozonation, Fenton, photo-Fenton, UV/H_2O_2, or combining UV with heterogeneous catalysts (e.g., TiO_2 and ZnO) [16]. The advantage of AOPs is not only to decolorize but also to mineralize toxic organic compounds into less toxic final products (e.g., CO_2 and H_2O), contributing to minimizing risks to human health and the environment. Among them, photocatalysis is receiving much attention from many scientists around the world, because of its high efficiency, low initial cost, is a simple process, and eco-friendliness [17].

Nowadays, many scientists synthesised the nanomaterials to treatment the pollutants in an aqueous environment. TiO_2 received much attention and research from scientists. Because it has low cost, easy synthesis, high redox potential, environmental friendliness, and photochemical stabilization. Many previous studies have shown the superior photocatalytic ability of TiO_2 in degrading organic pollutants in aquatic environments. In 2010, Sungmin Chin and associates successfully synthesized TiO2 nanoparticles by the thermal decomposition of titanium tetraisopropoxide [18]. The specific surface areas of the TiO_2 nanoparticles were more than 134.4 m^2/g and the photocatalytic activity for methylene blue was higher than that of the commercial photocatalyst. In 2020, TiO_2 nanoparticles were synthesized by Mohammad Malakootian and associates to degrade ciprofloxacin [19]. This material was highly pure and uniform in the size range of 39.2–74.9 nm. In the optimal conditions, the ciprofloxacin degradation efficiency achieved 86.57 %. However, to enhance recovery and reuse ability, many scientists doped TiO_2 nanoparticles onto the substrates such as activated carbon, silica, and graphene oxide.

However, a critical consideration in employing TiO_2 photocatalysis for water treatment is its environmental footprint and sustainability. Free TiO_2 nanoparticles in slurry reactors can be difficult to separate from treated water and pose risks of nanoparticle release into the environment, potentially causing secondary pollution. Photocatalytic processes also typically require intense UV/visible light irradiation, which entails significant energy consumption, and partial oxidation of complex pollutants may yield intermediate by-products that have residual toxicity. These factors have prompted comprehensive AOP evaluations highlighting the need to benchmark energy efficiency and control by-products when deploying photocatalytic treatments. Immobilizing TiO_2 on stable supports (such as cordierite in this study) offers several environmental benefits. The fixed catalyst can be easily recovered and reused, preventing catalyst nanoparticles from leaching into the water column. Unlike homogeneous AOPs like Fenton, which produce iron sludge, an immobilized TiO_2 system generates no sludge waste – the catalyst remains attached to its substrate. Furthermore, heterogeneous photocatalysts can often operate over a broad pH range without chemical additives, improving compatibility with real wastewaters. By combining energy-efficient light sources and immobilized catalyst designs, photocatalytic technology can be made more sustainable, minimizing secondary contamination and facilitating greener water treatment processes. These environmental considerations underscore the importance of the TiO_2–cordierite approach, which addresses nanoparticle recovery and reusability, aiming for an effective yet environmentally benign treatment solution.

In this study, the TiO_2 nanoparticles were synthesized by sol-gel method. Cordierite substrates were successfully synthesized from kaolin and several different materials. Then, TiO_2 nanoparticles were coated into cordierite substrates by dip-coating and spray-coating methods. Their characteristics were analyzed by some modern techniques. The photocatalytic ability of the as-synthesized materials was evaluated via degrading methyl orange (MO) in water under the irradiation of a Xenon lamp.

2. Materials and Methods

2.1 Materials and Characterizations

In this study, all chemicals were used directly without further refining including tetraisopropyl orthotitanate (TTIP), acetic acid, ascorbic acid (AA), ethylenediaminetetraacetic acid (EDTA), isopropyl alcohol (IPA), ethanol, polyetylen glycol (PEG), and methyl orange (MO), which were purchased from Merck. In addition, distilled water (DW) was used throughout the experiments.

An X-ray diffractometer (German) was used to determine the phase existence of TiO_2 with the 2θ range of 20 – 90 °. The morphology of the as-synthesized materials was observed by a scanning electron microscope (SEM JEOL serios 7600F), which was also equipped with EDS to determine the elemental composition. The N2 adsorption/desorption isotherms were analyzed at a bath temperature of 77.35 K, a low-pressure dose of 2.0 cm^3/g STP, an equilibrium interval of 10 s, and a sample density of 1.0 g/cm^3. A DR/UV-Vis spectrometer was used to measure the light absorption capacity of the synthesized materials.

2.2 Titanium Oxide (TiO_2) Synthesis Process

12.6 mL of TTIP 98 % and 50 mL of IPA 98 % were mixed and stirred to completely solute in a 100 mL beaker. This mixture was added to a beaker containing 25 mL acetic acid 99.5 % which was refrigerated by the ice and salt mixture and was stirred continuously. After that 140 mL of DW was gradually added to this above mixture and stirred to appear the white precipitate. After 1.5 h stir vigorously, this precipitate completely dissolved to obtained transparent sol. This sol was dried at 80 °C for 24 h and the grounded to obtain the gel powder. Finally, this gel powder was bake at different temperatures for 5 h with the heating rate of 2 °C/min to obtain the TiO_2 powder.

2.3 Cordierite Substrates Synthesis Process

The mixture including 100 g of kaolin, 10.24 g of MgO, 6.02 g of $Al(OH)_3$, and 23.5 g of dolomite was finely grounded and then stirred with DW for 12 h. After that this mixture was allowed to settle, decanted, and filtered to obtain a paste. Finally, this paste was created form with the size of 25×12×3 mm, dried at 120 °C for 3 h, and then bake at 950 °C for 5 h with the heating rate of 5 oC/min to obtain cordierite.

2.4 Process of Coating the TiO_2 Nanoparticles onto Cordierite Substrates

2.4.1 Dip-coating method

2 g of the gel powder was added to a beaker containing 30 mL of DW and PEG and then stirred evenly to obtain the mixture A. Cordierite was dried at 80 °C for 30 min and then dipped to the mixture A. After 5 min, cordierite was lifted out and dried at 80 °C for 30 min. This process was repeated 5 times. Finally, this cordierite was baked at 400 °C for 5 h with the heating rate of 2 °C/min to obtain TiO_2-coated cordierite, which was named TCC-Dip.

2.4.2 Spray-coating method

0.2 g of the gel powder and 12.5 mL of ethanol were added to 15 mL sample tube and shaken well. Then, this mixture was added to a sample cup mounted on spray gun body. Similar to dip-coating method, cordierite was dried at 80 °C for 30 min. After that cordierite was arranged onto a stand and fixed with double-sided tape. The stand was heated at 125 °C and the injection speed was 1 mL/min. This spray process was repeated many times. Finally, this cordierite was baked at 400 °C for 5 h with the heating rate of 2 °C/min to obtain TiO_2-coated cordierite, which was named TCC-Spray.

2.5 Methyl Orange (MO) Degradation Process

The photocatalytic ability of the as-synthesized materials was evaluated through the MO degradation efficiency in aqueous medium. The reaction conditions include the MO concentration of 20 mg/L, the catalyst dosage of 0.5 g/L, the 300 W Xenon lamp, and the temperature of 30 °C. Before beginning the photocatalytic process, the reaction beaker was stirred in dark for 30 min to achieve adsorption equilibrium. The time when the light starts to shine is considered the time when the photocatalytic process starts. After each certain period of time, the reaction sample was taken out and filtered to obtain the pure MO solution. This MO solution was analyzed by ultraviolet-visible spectrophotometry to determine the MO concentration. The Equations (1) and (2) were used to calculate the MO degradation efficiency and rate reaction [20-22].

$$Degradation\ efficiency\ (\%) = \frac{C_0 - C}{C_0} \times 100\% \quad (1)$$

$$-\ln\frac{C}{C_0} = k \times t \quad (2)$$

where, C and C_0 are the MO concentration at time t and $t = 0$, respectively, k is the rate reaction; t is the time.

3. Results and Discussion

3.1 The Optimal TiO_2 Nanoparticles Synthesis Condition

TiO_2 crystals exhibit three main phases: rutile, anatase, and brookite. Each phase possesses distinct properties, characteristics, and applications. Notably, anatase is the phase commonly utilized in wastewater treatment due to its exceptional photocatalytic properties. Depending on specific application objectives, different methods and synthesis conditions are employed to obtain the TiO_2 nanoparticles in the desired phase. In this study, the TiO_2 nanoparticles were synthesized using the sol-gel method and calcined at various temperatures (300, 350, 400, and 450 °C). This investigation of temperature aims to determine the optimal conditions for maximizing the TiO_2 nanoparticles in the anatase phase. In essence, the resulting the TiO_2 nanoparticles demonstrates superior photocatalytic capabilities.

The results of the characteristic analysis of the synthesized TiO_2 nanoparticles are presented in Figure 1, Table 1, and Table 2. Based on these results, the transition between the crystal phases of the TiO_2 nanoparticles can be objectively evaluated. From there, the optimal temperature conditions for the synthesis of the TiO_2 nanoparticles for photocatalytic applications can be determined. As shown in the XRD spectrum,

the synthesized TiO_2 nanoparticles primarily exist in the anatase and rutile phases, indicated as A and R, respectively, in Figure 1. At a calcination temperature of 300 °C, the TiO_2 nanoparticles exist in both phases (A and R), although the peaks characteristic of the R phase are very weak. When the calcination temperature was increased to 350 and 400 °C, the peaks of the R phase become nearly nonexistent. Thus, the calcination temperature significantly influences the phase existence of the TiO_2 nanoparticles. As the calcination temperature increased, the TiO_2 nanoparticles tended to transform from the R phase to the A phase. However, when the calcination temperature was raised to 450 °C, the phase transformation of the TiO_2 nanoparticles occurred in the opposite direction, with a significant increase in the amount of the R phase. This is clearly observed in the XRD spectrum of the TiO_2 nanoparticles at 450 °C. On the other hand, the percentage of each phase and the crystallite size of the synthesized TiO_2 nanoparticles are also presented in Table 1. According to Table 1, as the calcination temperature increased, the percentage of the A phase rose. When calcined at 300 °C, 94.47 % of the TiO_2 nanoparticles were in the A phase. Meanwhile, the percentage of the A phase increased to 97.44 % when the TiO_2 nanoparticles were calcined at 400 °C. Furthermore, diffraction peaks can also characterize crystal size, crystallinity, and preferential orientation. As shown in Figure 1, the XRD diffraction peak intensity of TiO_2 calcined at 400 °C was lower than that of samples calcined at 300 and 350 °C, but the width of the diffraction peak increases (broadens). This led to the crystallite size of the TiO_2 nanoparticles tended to decrease as the calcination temperature increased (following the Scherrer equation $D = K \lambda / \beta \cos \theta$ [20]). The crystallite size of the TiO_2 calcinated at 300 and 350 °C was 4.86 and 4.83 nm, which was larger than that of the TiO_2 calcinated at 400 °C (D = 4.80 nm), as shown in Table 1. In addition, these results indicated that the crystallinity of the TiO_2 calcinated at 300 and 350 °C was better than that of the TiO_2 calcinated at 400 °C. Notably, the percentage of the A phase sharply declined when the TiO_2 nanoparticles were calcined at 450 °C, dropping to 83.79 %, and the crystal size also increased slightly to 4.92 nm. Additionally, no strange diffraction peaks were observed, proving that the synthesized TiO_2 nanomaterials were of high purity (containing no impurities). The SEM analysis was conducted to investigate the effect of calcination temperature on the morphology and particle size of the TiO_2 nanomaterials. According to Figure 2, the SEM images showed clearly that the calcination temperature did not influence the morphology of the synthesized TiO_2 nanomaterials, which retain their irregular spherical shapes. However, the particle size significantly changed, especially that of the TiO_2 nanomaterial at 450 °C was larger, as shown in Figure 2(d), consistent with the XRD analysis results.

In addition to the phase and crystal size, the pore size and surface area of the TiO_2 nanoparticles are also important factors affecting their photocatalytic process. Table 2 presents the research results regarding these factors for the synthesized TiO_2 nanoparticles. It is evident that the pores and surface area of the TiO_2 nanoparticles are significantly dependent on their calcination temperature. As the calcination temperature of the TiO_2 nanoparticles increased, both the pore size and surface area tend to rose.

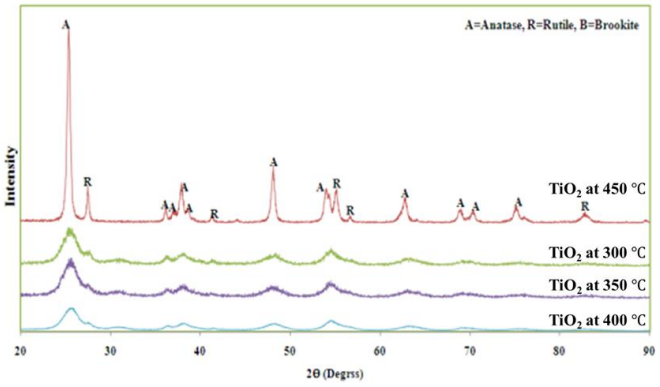

Figure 1. XRD pattern of synthesized TiO_2 nanoparticles.

Table 1. Percentage of anatase phase and crystal size of synthesized TiO_2 nanoparticles.

Samples	Anatase phase (%)	Crystal size (nm)
TiO_2 at 300 °C	94.47	4.86
TiO_2 at 350 °C	95.07	4.83
TiO_2 at 400 °C	97.44	4.80
TiO_2 at 450 °C	83.79	4.92

Table 2. Textural properties of the synthesised TiO_2 nanoparticles.

Samples	TiO_2 at 300 °C	TiO_2 at 350 °C	TiO_2 at 400 °C	TiO_2 at 450 °C
Surface area (m^2/g)	144	155	160	139
Pore volume (cm^3/g)	0.048	0.097	0.069	0.047
Pore size (Å)	45	152	150	128

For instance, the TiO_2 nanoparticles calcined at 300 °C have a surface area and pore size of 144 m^2/g and 45 Å, respectively. Conversely, when the calcination temperature reaches 400 °C, both the surface area and pore size increased to 160 m^2/g and 150 Å, respectively. However, at a calcination temperature of 450 °C, the surface area and the pore size decreased, as shown in Table 2. Based on the results of the characteristic analysis of the synthesized TiO_2 nanoparticles, it can be seen that the TiO_2 nanoparticles synthesized at 400 °C exist in the A phase the most and also have the largest surface area. Therefore, these TiO_2 nanoparticles can be predicted to have the best photocatalytic capacity.

The band gap energy (E_g) is very important in photocatalysis, because it determines the ability to absorb light and the efficiency of the catalytic process. Figure 3 shows the DR/UV-Vis spectra and Tauc's plots of the synthesized TiO_2 nanomaterials. All nanomaterials strongly absorbed light in the UV region, especially in the wavelength range of 250-325 nm; this significantly decreased in the wavelength range of 325-425 nm, as shown in Figure 3(a). Additionally, all nanomaterials showed stability at the wavelengths above 425 nm. Moreover, the Eg values of these nanomaterials were calculated by Tauc's equation ($(\alpha h\nu)^{1/n} = A(h\nu - E_g)$ [20]). The band gap energy of the synthesized TiO_2 nanomaterials vary from 3.26 to 3.21 eV, as shown in Figure 3(b). According to the previous studies, the band gap decreases when the rutile phase percent increases [23,24]. The E_g value of the TiO_2 nanomaterial calcinated at 300 °C increased from

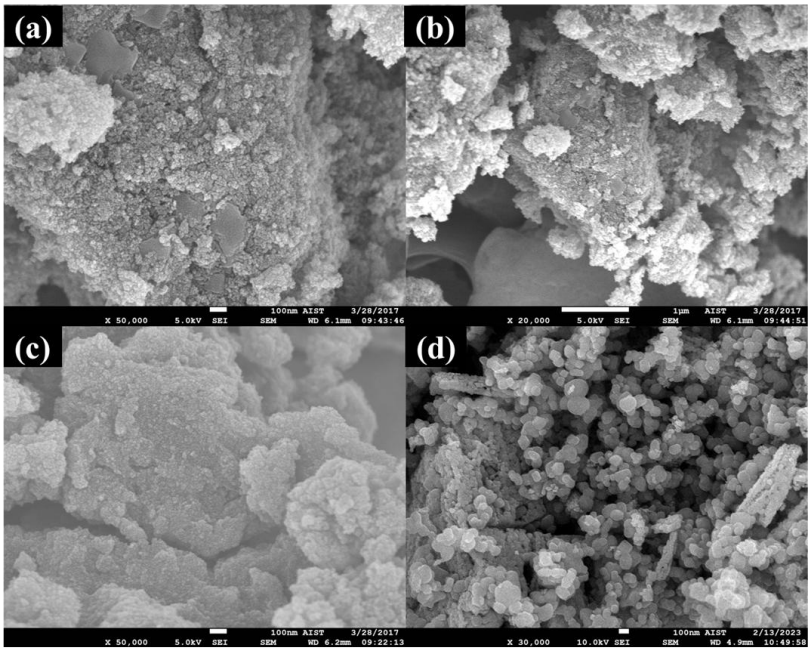

Figure 2. The SEM images of the synthesized TiO_2 nanomaterials at (a) 300, (b) 350, (c) 400, and (d) 450 °C.

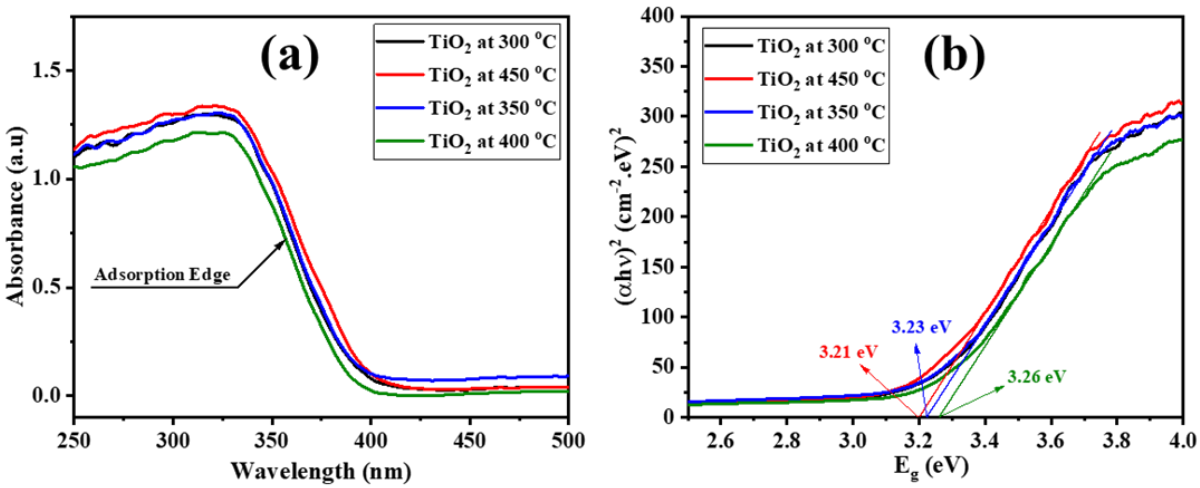

Figure 3. (a) The DR/UV-Vis spectra and (b) Tauc plots of the synthesized TiO_2 nanomaterials.

3.23 to 3.26 eV (at 400 °C), when the rutile phase percent decreased by the XRD analysis results. Especially, the Eg value significantly decreased, which just achieved about 3.21 eV (at 450 °C), when the rutile phase percent strongly increased, as shown in Table 1. These differences can be explained based on the difference in the crystalline size. For most semiconductors, a decrease in the band gap energy with an increase in the crystalline size leads to a red shift of the optical absorption edge [25], consistent with these results in this study.

In addition to evaluating the characteristics of the synthesized TiO_2 nanoparticles, experimental assessments were also performed and presented in this study. The photocatalytic activity of the synthesized TiO_2 nanoparticles was evaluated based on their Methyl Orange (MO) degradation efficiency. The reaction conditions include the MO concentration of 20 mg/L, the catalyst dosage of 0.5 g/L, the 300 W Xenon lamp, the temperature of 30 °C, and t = 360 min. The experimental results are presented in Figure 4. In general, the synthesized TiO_2 nanoparticles can degrade MO with a degradation efficiency exceeding 65 %. However, each type achieved different degradation efficiencies. Notably, the TiO_2 nanoparticles synthesized at 400 °C exhibited significantly better photocatalytic capacity than the other nanoparticles, with the MO degradation efficiency of 95.97 %. Therefore, the experimental results once again confirmed that the TiO_2 nanoparticles synthesized at 400 °C possess the best photocatalytic capacity. Based on the research results, 400 °C was selected as the optimal calcination temperature for synthesizing TiO_2 nanoparticles and applied in further studies.

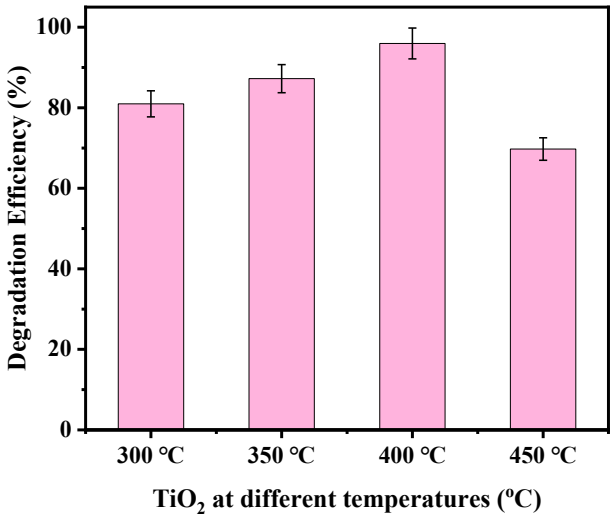

Figure 4. The MO degradation efficiency of the synthesized TiO_2 nanoparticles.

3.2 Photocatalytic Activity of the TiO_2 Nanoparticles Coated on Cordierite.

3.2.1. Characteristics

In this study, TiO_2 nanoparticles were coated onto cordierite using spray and dip methods, referred to as TCC-Spray and TCC-Dip, respectively. Before evaluating the photocatalytic activity of these materials, their characteristic properties were investigated. The morphology of these materials can be observed based on the SEM analysis results presented in Figure 5(a-b). In the spraying method, the TiO_2 nanoparticles exhibit relatively uniform sizes, agglomerating into clusters to create a porous structure, as shown in Figure 5(a). In contrast, for the dipping method, the TiO_2 nanoparticles display uneven sizes and are arranged in a disorderly manner, as illustrated in Figure 5(b). This difference in morphology also contributes to the variation in the photocatalytic capacity of these materials. Furthermore, the EDS analysis results indicated that TiO_2 nanoparticles were relatively tightly adhered to the surface of cordierite. The signals of the elements (Mg, Al, and Si) in the cordierite composition were very weak, as shown in Figure 5(c). The mass and atomic percentages of each element are specifically presented in Table 3. Ti and O were the two main elements identified, with mass percentages of about 86.57 – 88.52 and 9.99 - 10.43 %, respectively. Based on, the EDS results of the TCC – Spray and TCC – Dip can relatively concluded that the amount of TiO_2 nanomaterials coated on the cordierite surface by two methods was almost the same. Other elements, such as Mg, Al, Si, and S, accounted for less than 1 %, indicating that the process of coating TiO_2 nanoparticles onto cordierite was smooth and

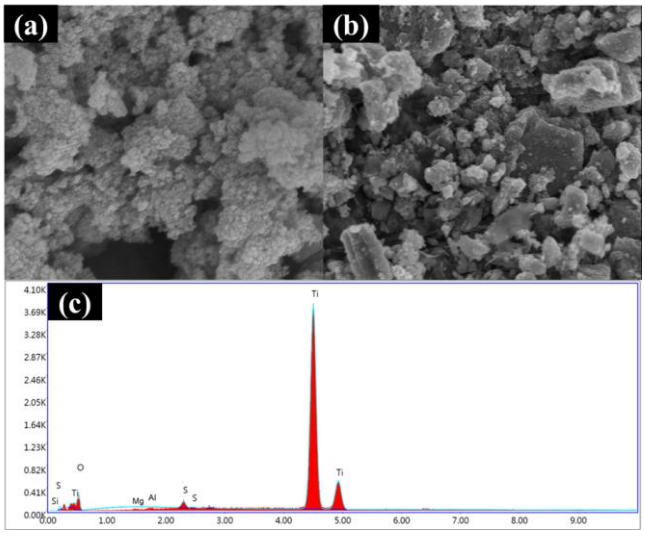

Figure 5. The SEM images of (a) TCC – Spray and (b) TCC – Dip, and (c) the EDS result of the TCC - Dip.

highly effective. Especially, the content of these elements was very low in the TCC – Spray, which just achieved from 0.19 to 0.42 % (lower than TCC – Dip), indicating that the spray coating method can coat the TiO_2 nanomaterials better and more evenly on the cordierite surface.

On the other hand, the surface area, pore volume, and pore size of these materials were also studied and evaluated. The results are presented in detail in Table 4. These findings indicate that the coating method significantly affects the formation of pores on the material surface. The pore size and volume of TCC-Dip were only 143 Å and 0.047 cm^3/g, respectively. When using the spray method (TCC-Spray), the pore size increase significantly (the pore size of 151 Å) and the pore volume (0.032 cm^3/g) tends to decrease. In particular, the surface area of TCC-Spray (136 m^2/g) was larger than that of TCC-Dip (128 m^2/g). Based on the results of the characteristic analysis of the materials, it can be predicted that TCC-Spray will have better adsorption and photocatalytic properties than TCC-Dip.

3.2.2. Photocatalytic activity

The adsorption capacity of the materials was evaluated under conditions including the initial MO concentration of 20 mg/L, a temperature of 30 °C, a duration of 120 min, and in the dark. As shown in Figure 6(a), TCC-Spray exhibited a higher adsorption efficiency than TCC-Dip. During the 120 min, the MO adsorption efficiency of TCC-Spray reached 13.41 %, while TCC-Dip only achieved 11.45 %. Notably, after 30 min of adsorption, the MO adsorption efficiency of the materials remained almost constant. This indicates that after 30 min, adsorption equilibrium was established, and this time point was also used in subsequent studies.

After the adsorption process, the catalytic process was performed under a 300 W Xenon lamp. After every 2 h of illumination, the reaction sample was retrieved, and the concentration of MO was determined. The MO degradation efficiency evaluation results are presented in Figure 6(b). It is evident that after 2 h of illumination, TCC-Spray achieved an MO degradation efficiency of 37.98 %, while TCC-Dip only reached 20.03 % (a difference of about 18 %). Initially, it can be assessed that TCC-Spray has a better photocatalytic ability than TCC-Dip. After 8 h, the MO degradation efficiency of both TCC-Spray and TCC-Dip increased significantly to 94.12 and 78.99 %, respectively. Notably, after 10 h of illumination, TCC-Spray nearly completely degraded MO (20 mg/L).

Additionally, the first-order kinetic equation was applied, and the rate of MO degradation of the as-synthesized materials was evaluated. As shown in Figure 7, it can be observed that the first-order kinetic model fits the MO degradation process completely, with R^2 values all approximately equal to 1. This result also

Table 3. The EDS result of coated TiO_2 nanoparticles on cordierite.

Element	TCC - Dip		TCC - Spray	
	Weight %	Atomic %	Weight %	Atomic %
O	9.99	25.14	10.43	26.09
Si	0.89	1.01	0.23	0.38
S	0.96	1.17	0.42	0.46
Mg	0.76	0.81	0.19	0.22
Al	0.83	0.92	0.21	0.34
Ti	86.57	70.95	88.52	72.51

Table 4. Textural properties of TCC – Spray and TCC – Dip.

Properties	TCC-Dip	TCC-Spray
Surface area (m^2/g)	128	136
Pore volume (cm^3/g)	0.047	0.032
Pore size (Å)	143	151

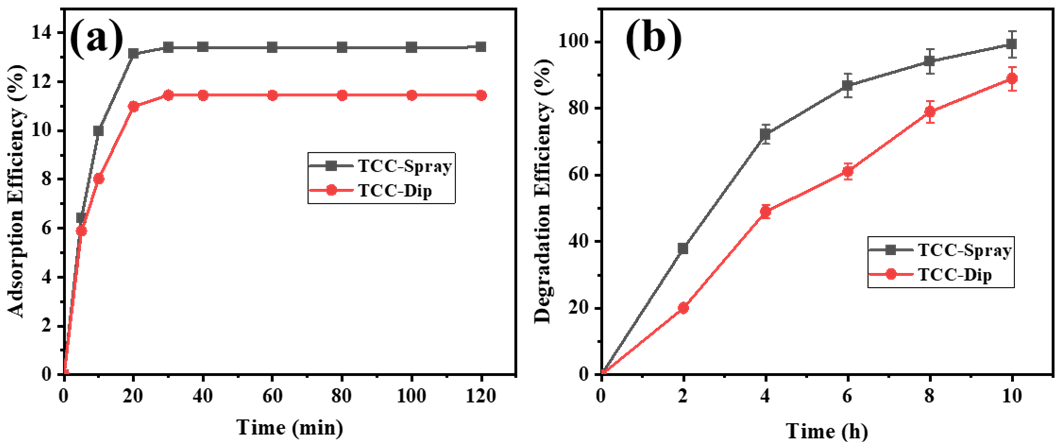

Figure 6. The MO (a) adsorption and (b) degradation efficiency of TCC – Spray and TCC – Dip.

indicates that TCC-Spray has an MO degradation rate nearly twice as fast as that of TCC-Dip. The difference in photocatalytic ability of the materials can be attributed to the higher specific surface area of TCC-Spray compared to that of TCC-Dip, which leads to better interaction between MO molecules and the material surface. In conclusion, from the above results, it can be confirmed that the spray coating method facilitates uniform coverage of TiO_2 nanoparticles on the surface of cordierite with relatively uniform size, resulting in a larger surface area, greater adsorption capacity, and significantly enhanced photocatalytic activity compared to the dip coating method.

3.2.3. Photocatalytic mechanism

The photocatalytic mechanism is simulated as Figure 8 and proposed as follows: When an energy source larger than the band gap energy of TiO_2 nanoparticles is irradiated on the surface of the material, electrons (e^-) transfer from valence band (VB) to conduction band (CB), simultaneously creating holes (h^+) at VB. At CB, the e^- combine with O_2 dissolved in water to form •OH radicals as shown in Figure 8. Meanwhile, at VB, the holes also combines with OH- in water to form •OH radicals. Then, MO molecules react with •OH radicals to form intermediate products through oxidation, mineralization, etc. Finally, these intermediate products will be completely converted into harmless substances such as CO_2, H_2O, NH_3, NH_4^+, and Na^+. Some of the reactions occurring during MO decomposition are proposed as shown in Figure 8.

In photocatalytic systems like TiO_2, hydroxyl radicals (•OH), superoxide radicals ($•O_2^-$), and photogenerated holes (h^+) are typically the primary oxidizing agents. For example, in a recent work by Hassani *et al.* on an mpg-C_3N_4/Ag/ZnO nanowires/Zn photocatalyst, the introduction of various scavengers revealed that •OH and h^+ were the primary species responsible for dye degradation [26]. In similar studies on advanced photocatalysts, researchers have used specific scavengers to confirm this. For example, adding ethylenediaminetetraacetic acid (EDTA), a well-known hole (h^+) scavenger, greatly reduced dye degradation efficiency, indicating that holes play a crucial role. Likewise, isopropyl alcohol (scavengers for •OH) typically causes a sharp decrease in degradation rates, confirming •OH as a main active species. Finally, ascorbic acid (AA) is the scavenger for $•O_2^-$. To validate the proposed photocatalytic mechanism and identify the reactive oxygen species involved in MO degradation, some reactive species scavenging experiments were performed, similar to the previous study [22]. According to Figure 9, the MO degradation efficiency decreased sharply in the presence of radical scavengers (including EDTA and AA), confirming that •OH and $•O_2^-$ radicals were the two primary oxidizing agents in the MO degradation process of TiO_2 nanomaterials.

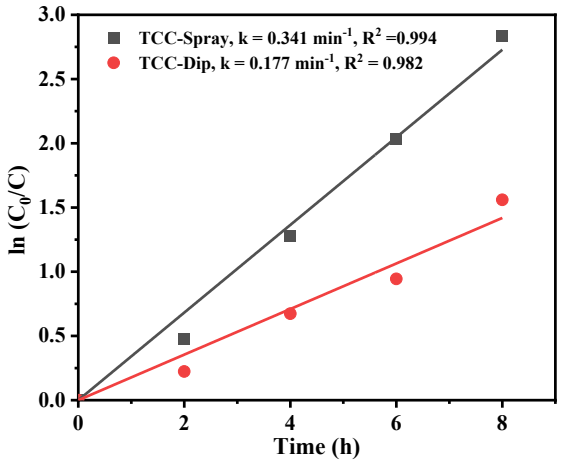

Figure 7. The kinetic curves of TCC – Spray and TCC – Dip.

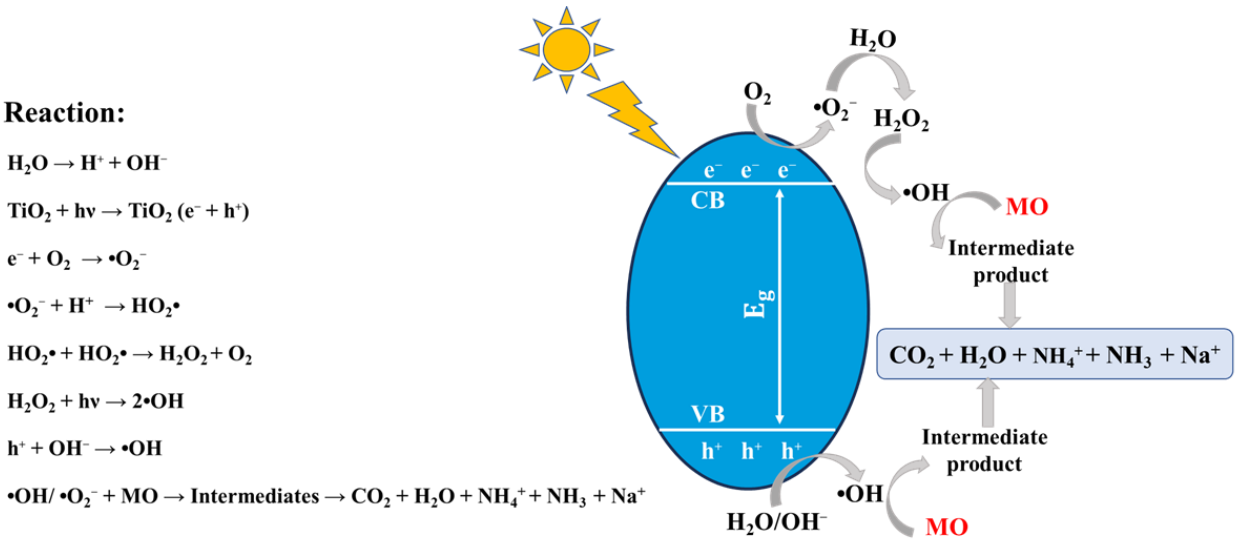

Figure 8. Photocatalytic mechanism.

3.3 Comparison of TiO_2 Powder and TiO_2 Coating

In this study, the MO degradation efficiency of TiO_2 powder and TiO_2 coating was evaluated and compared. As shown in Figure 10, the MO degradation efficiency of TiO_2 powder was significantly superior to that of TiO_2 coating. After 2 h, the MO degradation efficiency reached 48.43 %, which was 10 and 28 % higher than that of TCC-Spray and TCC-Dip, respectively. Notably, after only 6 h, MO was almost completely degraded, while TCC-Spray and TCC-Dip had degradation efficiencies of only 86.87 and 61.09 %, respectively. Thus, it is clear that TiO_2 powder has better photocatalytic ability than TiO_2 coating. This can be explained by the fact that TiO_2 powder is easily dispersed evenly in the MO solution, leading to better interaction between MO molecules and the surface of TiO_2 nanoparticles, resulting in high degradation efficiency. However, TiO_2 powder is limited in terms of recovery and reuse after each photocatalytic treatment cycle. To ensure the most objective evaluation results, the experiments to assess the recovery ability of the materials were carried out under the following conditions: MO concentration of 20 mg/L, time of 600 min, temperature of 30 °C, and a 300 W Xenon lamp. The evaluation results after 5 treatment cycles are presented in Figure 11. Based on these results, it is evident that TiO_2 powder has very poor recovery and reuse ability compared to TiO_2 coating. After 5 cycles, the MO degradation efficiency sharply decreased from 100 to 49.09 %. This indicates that the recovery of TiO_2

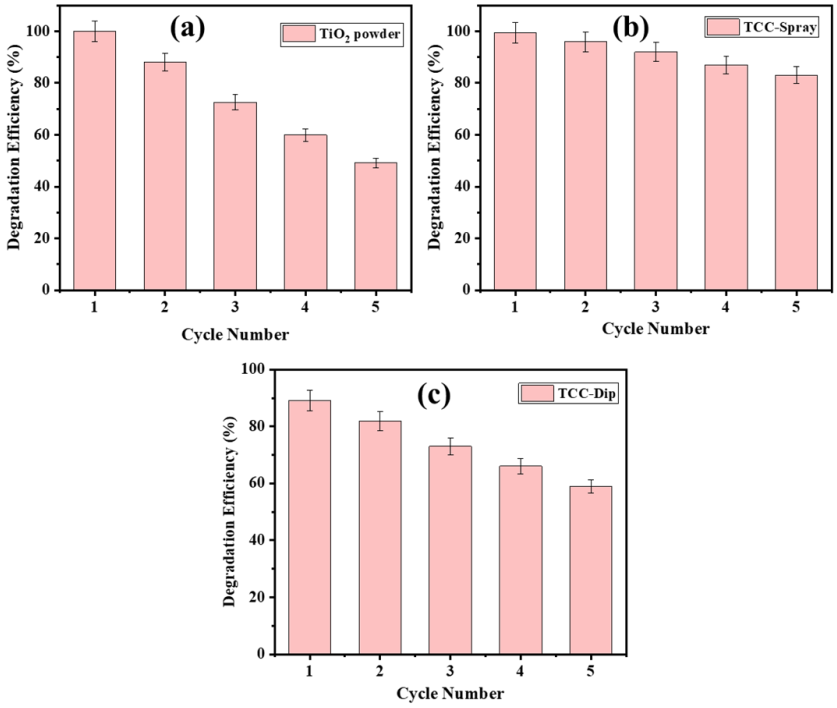

Figure 11. The MO degradation efficiency of the as-synthesized materials with five cycles.

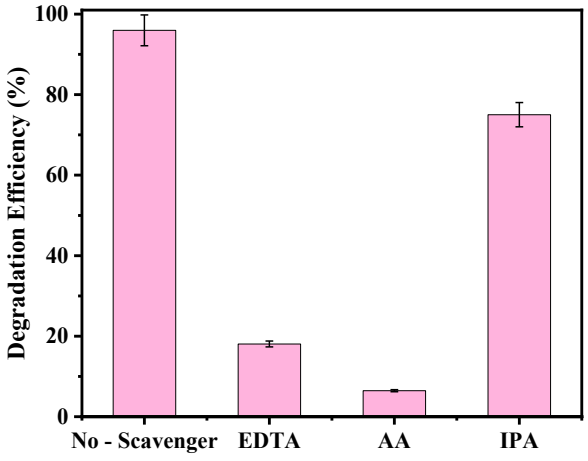

Figure 9. Effects of the different scavengers on the MO degradation efficiency.

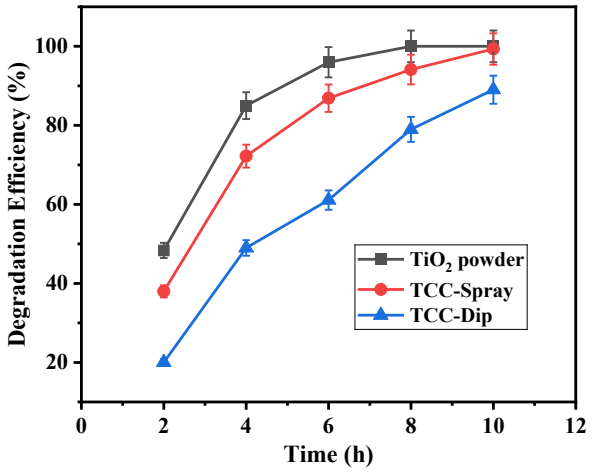

Figure 10. The MO degradation efficiency of TiO_2 powder, TCC – Spray, and TCC – Dip.

nanoparticles is a significant challenge. Therefore, coating TiO_2 nanoparticles on substrates is a promising method to enhance their recovery and reuse ability. The results of the MO degradation efficiency evaluation of TiO_2 coatings met expectations, as shown in Figure 11(b-c). It is observed that the MO degradation efficiency of the material exceeds 55 % after 5 reuse cycles. In particular, TCC-Spray demonstrates a much better recovery ability; after 5 cycles, the MO degradation efficiency still reaches 83.07 %. A significant decrease in the activity of the TiO_2 powder after many cycles can be attributed to several reasons. During the reuse process, the gradual decrease of the TiO_2 nanoparticles with each cycle can be the main cause of this deterioration. Moreover, the specific surface area decreased significantly after 5 reuse cycles, which only reached 98 m^2/g, as shown in Table 5. In particular, the change in pore structure was clearly shown through the reduction in size as well as volume. These lead to a reduction in the available active sites on the surface of the TiO_2 nanomaterial and the interaction between this nanomaterial and the MO molecules, leading to a reduction in the MO degradation activity of the TiO_2 nanomaterial after many cycles. Thus, based on the research findings, it can be concluded that TCC-Spray exhibits the best photocatalytic and recovery ability, which is a promising and potential material in the field of wastewater treatment.

3.4 Comparison with the Previous Studies

Due to the potential adverse effects of MO on human health and ecology, scientists worldwide have studied various catalytic materials for MO degradation in aquatic environments [27-33]. This study lists and presents a series of investigations on MO degradation in Table 6. Evaluating and comparing the MO degradation capabilities of these materials is challenging because each study employed different conditions during the degradation process. However, the materials have been assessed and compared as objectively as possible. Each material exhibits different MO degradation efficiencies, all achieving over 85 %. Although these materials have superior capabilities for degrading MO, they are limited in recovery and reuse due to their powder form. In contrast, the TiO_2 nanoparticles coated on cordierite in this study demonstrate high recovery and reuse potential. Notably, TiO_2 nanoparticles coated using the spray method (TCC-Spray) exhibit the most remarkable recovery and reuse ability.

Table 5. Textural properties of the TiO_2 nanoparticles before and after using the MO degradation.

Samples	TiO_2 powder - fresh	TiO_2 powder - used
Surface area (m^2/g)	160	98
Pore volume (cm^3/g)	0.069	0.031
Pore size (Å)	150	38

To apply the TiO_2 - cordierite photocatalytic process in a real context, it is useful to compare its advantages and limitations with other advanced oxidation processes. One clear advantage of this heterogeneous photocatalysis system is the absence of sludge generation. In Fenton and photo-Fenton AOPs, the reaction inherently produces ferric hydroxide sludge (due to Fe^{3+} formation and neutralization), which adds a significant burden of separation and disposal. On the other hand, TiO_2–cordierite is a zero-sludge process, and the only solids present are the catalyst pieces, which are easily recovered, and no additional chemicals are introduced that would form residual waste. The ease of catalyst recovery is another strong point: the cordierite can be simply taken out of the reactor, whereas in homogeneous processes like Fenton or ozone, the dissolved catalysts or ozone must be quenched, and there is no reusable component to recover. In summary, TiO_2–cordierite photocatalysis offers key benefits, including no sludge generation and easy catalyst recovery. Each AOP has its niche: for instance, Fenton might achieve very rapid degradation for certain pollutants in controlled conditions, and ozone is very effective for disinfection and certain micropollutants. However, the immobilized TiO_2 approach aligns well with sustainable treatment goals by emphasizing reusability and minimal secondary waste. In practice, hybrid treatment trains can capitalize on these differences; for example, one could use TiO_2 photocatalysis as a first stage to break down dye molecules and then a Fenton or biological process as a second stage to polish off remaining intermediates. Such combinations (photocatalysis and Fenton or photocatalysis and biodegradation) are increasingly reported to achieve complete mineralization and detoxification of textile effluents more efficiently than single processes. The findings of this study suggest that TiO_2–cordierite could be a strong candidate for the photocatalytic component in a multi-step water treatment scheme, offering easy integration and retrieval. Overall, positioning TiO_2–cordierite among AOPs highlights its role in achieving high pollutant removal with operational simplicity and environmental safety.

4. Conclusion

In summary, TiO_2 nanoparticles were synthesized using the sol-gel method with varying calcination temperatures. When calcined at 400

°C, 97.44 % of the synthesized TiO_2 nanoparticles were in the anatase phase. These nanoparticles exhibited a surface area and pore size of 160 m²/g and 150 Å, respectively. Additionally, these TiO_2 nanoparticles demonstrated the highest photocatalytic activity, achieving an MO degradation efficiency of 95.97 % in 360 min. Therefore, 400 °C was established as the optimal calcination temperature for processing the coated TiO_2 materials. After being coated on cordierite, the catalytic performance of TiO_2 nanoparticles showed a tendency to decrease; however, their recovery and reuse capabilities were significantly enhanced. Notably, TCC-Spray exhibited a much higher MO degradation efficiency along with superior recovery and reuse ability compared to TCC-Dip. After five reuse cycles, the MO degradation efficiency still reached 83.07 %. TCC-Spray is a promising material with extensive applications in wastewater treatment. Thus, TiO_2 nanoparticles coated on cordierite demonstrate much better recovery and reuse capabilities than TiO_2 powder. In conclusion, the spray coating method is the most effective technique for applying TiO_2 nanoparticles onto cordierite.

Moving forward, this study will be extended to investigate the optimal conditions for MO degradation process and exploring the long-term stability of the TiO_2-coated cordierite under real wastewater conditions could provide valuable insights for practical applications. Moreover, several avenues can be explored to further enhance the performance and applicability of the TiO_2–cordierite system. One approach is to develop Z-scheme heterojunctions on the cordierite support by coupling TiO_2 with a visible-light-responsive semiconductor. For example, integrating graphitic carbon nitride (g-C_3N_4) or a narrow-band-gap oxide/sulfide (such as AgI, BiOBr, or WO_3) with TiO_2 in a direct Z-scheme configuration could extend the photoresponse into the visible range while maintaining strong oxidizing power. Another promising direction is to incorporate layered double hydroxides (LDHs) or other adsorptive components as interlayers or co-catalysts on the cordierite. As discussed, LDHs can pre-concentrate anionic dyes (like MO) from solution via anion exchange, bringing the pollutant into proximity with the photocatalyst surface. A TiO_2–LDH bilayer or hybrid coating could thus combine the strong adsorption capacity of LDHs with the oxidative degradation by the TiO_2 nanomaterial, potentially achieving faster or more complete mineralization than the pure TiO_2 nanomaterial. Additionally, LDHs often impart alkalinity and could help buffer local pH, which might benefit processes that generate acids upon pollutant mineralization. Future work could

Table 6. Textural properties of the TiO_2 nanoparticles before and after using the MO degradation.

Catalyst	Photocatalysis conditions	Degradation Efficiency (%)	Reference
Pd-TiO_2	[MO] = 20 mg/L, [Pd-TiO_2] = 10 mg/L, T = 25 ℃, t = 120 min, and a 100 W high pressure mercury lamp	92.6	[29]
La-doped ZnO	[MO] = 10 mg/L, [La-doped ZnO] = 0.5 g/L, t = 150 min, and visible light irradiation	85.86	[31]
Activated Carbon/ZnO	[MO] = 10 mg/L, [Activated Carbon/ZnO] = 0.2 g/L, pH = 6, t = 180 min, and a UV lamp	90.00	[28]
Au-ZnO	[MO] = 10 mg/L, [Au-ZnO] = 0.1 g/L, t = 140 min, and UV irradiation	94.90	[27]
ZnO-Al_2O_3-CeO_2-Ce_2O_3	[MO] = 40 mg/L, [ZnO-Al_2O_3-CeO_2-Ce_2O_3] = 0.02 g/L, t = 300 min, and a 250 W mercury lamp	99.80	[33]
Pt-NiO-ZnO hybrids	[MO] = 10 mg/L, [Pt-NiO-ZnO hybrids] = 0.04 g/L, and t = 120 min	98.40	[32]
ZnO/Graphene Oxide	[MO] = 10 mg/L, [ZnO/Graphene Oxide] = 1.0 g/L, t = 120 min, and UV irradiation	95.00	[30]
TiO_2 powder	[MO] = 20 mg/L, T = 30 ℃, t = 480 min, and a 300 W Xenon lamp	100	This study
TCC-Spray	[MO] = 20 mg/L, T = 30 ℃, t = 600 min, and a 300 W Xenon lamp	99.32	This study
TCC-Dip	[MO] = 20 mg/L, T = 30 ℃, t = 600 min, and a 300 W Xenon lamp	89.02	This study

involve synthesizing an LDH (e.g., Mg-Al or Zn-Fe LDH) on the cordierite first, then depositing TiO_2 on top, to evaluate the synergistic effect on dye removal.

Acknowledgments

The authors express their sincere gratitude to Hanoi University of Science and Technology for its financial support, research facilities, and environment under the research project T2023-PC-052. The work was carried out at the Laboratory of Catalysis under the RoHan Project, funded by the German Academic Exchange Service (DAAD, No. 57315854) and the Federal Ministry for Economic Cooperation and Development (BMZ) through the "SDG Bilateral Graduate School Program".

CRedit Author Statement

Author Contributions: All authors contributed to the study conception and design.Trung Hieu Nguyen is the person who came up with the idea and is mainly responsible for this research. Minh Thang Le was the person who supported, advised, and reviewed during the study process. Trung Hieu Nguyen, Thu Huong Nguyen, and Anh-Tuan Vu performed material preparation, data collection, and analysis. Trung Hieu Nguyen wrote the first draft of the manuscript, and all authors commented on previous versions of the manuscript. All authors have read and agreed to the published version of the manuscript.

References

[1] Nguyen, T.H., Thi, M.L.V., Tran, T.P., Vu, A.-T. (2024). Modificstion of Porous Silica from Rice Husk with EDTA to Remove Pb2+ Ions in an Aqueous Environments. *Valorization of Agricultural Residues*, 60, 60-62, DOI: 10.14279/depositonce-21556

[2] Nguyen, T.H., Vu, A.-T. (2025). Preparation of novel B/ZnO/zeolite nanocomposites by simple combustion method for enhanced dye removal in an aqueous environment. *Nanotechnology*, 36(10), 105703. DOI: 10.1088/1361-6528/ada29b

[3] Vu, A.-T., Nguyen, T.H., Nguyen, T.H. (2023). Preparation of carnation-like Ag-ZnO composites for enhanced photocatalysis under visible light. *Nanotechnology*, 34(27), 275602. DOI: 10.1088/1361-6528/acca24

[4] Nguyen, T.H., Mai, T.T., Tran, T.P., Thi, C.L.T., Thi, C.V.D., Thi, M.L.V., Nguyen, M.V., Nguyen, T.H., Vu, A.-T. (2024). Studying the Nanocomposite B/ZnO for Photocatalysis: Facile Control the Morphology via Sol-gel Method and Antibiotic Degradation Investigations. *Journal of Sol-Gel Science and Technology*, 110(2), 319-332. DOI: 10.21203/rs.3.rs-3901804/v1

[5] Nguyen, T.H., Nguyen, V., Vu, A. (2024). Synthesis of CS-Fe3O4/GO nanocomposite for adsorption of heavy metal in aqueous environment. *Nanotechnology*. 35(34), 345705. DOI: 10.1088/1361-6528/ad50e3

[6] Nguyen, T.H., Vu, T.C., Le, T.P., Nguyen, T.H., Do, X.T., Vu, A.-T. (2024). Synthesis of Mesoporous ZnO‧ SiO2 Nanocomposite from Rice Husk for Enhanced Degradation of Organic Substances Including Janus Green B under Visible Light. *Bulletin of Chemical Reaction Engineering & Catalysis*, 19 (3), 429-441. DOI: 10.9767/bcrec.20175

[7] Nguyen, T.H., Vo, Q.L., Nguyen, N.T., Le, D.T., Tran, T.T.H., Nguyen, M.V., Le, V.D., Tran, V.H., Vu, A.-T. (2024). Fabrication of Graphene Oxide for Application in Removing Tetracycline Hydrochloride in Aqueous Solution. *JST: Engineering Technology for Sustainable Development*, 34(3), 8-15. DOI: 10.51316/jst.175.etsd.2024.34.3.2

[8] Nguyen, T.H., Nguyen, T.H., Nguyen, T.N., Nghiem, X.S., Le Minh, T., Vu, A.-T. (2025). Preparation of Functional Materials Based on Activated Carbon from Bagasse and Its Application in Pb2+ Adsorption in an Aqueous Environment. *Materials Today Communications*, 47, 113158. DOI: 10.1016/j.mtcomm.2025.113158

[9] Nguyen, T.M., Dao, T.C.V., Nguyen, T.H., Vu, T.C., Le, T.P., Nguyen, T.H., Vu, A.-T. (2024). Production of Porous Silica from Rice Husk Using Cetyltrimethylammonium Bromide to Remove Dyes in Aqueous Solution. *JST: Engineering Technology for Sustainable Development*, 34(4), 9-16. DOI: 10.51316/jst.177.etsd.2024.34.4.2

[10] Huong, N.T., Linh, V.Q., Thinh, N.N., Huyen, T.T.T., Viet, N.M., Hoang, T.V., Vu, A.-T. (2024). Assessment of the adsorption capacity tetracycline hydrochloride antibiotic in wastewater of graphene oxide materials. *Vietnam Journal of Catalysis and Adsorption*, 13(1), 87-92. DOI: 10.62239/jca.2024.014

[11] Nguyen, V.D., Nguyen, M.T., Vu, A.-T. (2024). Production of green biosorbent from chemically modified moringa leaves for enhanced removal of heavy metal in aqueous environment. *Biomass Conversion Biorefinery*, 15 (9), 1-21. DOI: 10.1007/s13399-024-06164-2

[12] Tuan, V.A., Huong, N.T., Viet, N.M. (2024). Novel B/ZnO material for enhanced degradation of tetracycline hydrochloride in an aqueous environment under visible light. *HaUI Journal of Science and Technology*, 60(3), 43-50, DOI: http://doi.org/10.57001/huih5804.2024.096.

[13] Vu, A.-T., Minh, P.Q., Anh, N.T.T., Vi, Đ.T.C., Hằng, N.T.B., Hương, N.T. (2024). Tổng hợp vật liệu Ag/ZnO/g-C3N4 bằng phương pháp nung đơn giản để loại bỏ kháng sinh tetracycline hydrochloride trong môi trường nước. *Journal of Control Vaccines Biologicals*, 4(1). DOI: 10.56086/jcvb.v4i1.142

[14] Vu, A.-T., Nguyen, M.V., Nguyen, T.H. (2024). Fabrication of ethylenediaminetetraacetic modified porous silica composite from rice husk for enhancing the remove of Pb2+ from aqueous solution. *Results in Materials*, 21, 100525. DOI: 10.1016/j.rinma.2023.100525

[15] Hassani, A., Motlagh, P.Y., Khataee, A. (2023). Hybrids layered double hydroxides as catalysts for the removal of synthetic dyes from wastewater, in *Current Developments in Bioengineering and Biotechnology*, 111-153. DOI: 10.1016/B978-0-323-91235-8.00020-6

[16] Hamdaoui, O. (2024) Innovative and Hybrid Advanced Oxidation Processes for Water Treatment. Elsevier.

[17] Hassani, A., Krishnan, S., Scaria, J., Eghbali, P., Nidheesh, P. (2021). Z-scheme photocatalysts for visible-light-driven pollutants degradation: a review on recent advancements. *Current Opinion in Solid State Materials Science*, 25(5), 100941. DOI: 10.1016/j.cossms.2021.100941

[18] Chin, S., Park, E., Kim, M., Jurng, J. (2010). Photocatalytic degradation of methylene blue with TiO2 nanoparticles prepared by a thermal decomposition process. *Powder Technology*, 201 (2), 171-176. DOI: 10.1016/j.powtec.2010.03.034

[19] Malakootian, M., Nasiri, A., Amiri Gharaghani, M. (2020). Photocatalytic degradation of ciprofloxacin antibiotic by TiO2 nanoparticles immobilized on a glass plate. *Chemical Engineering Communications*, 207(1), 56-72. DOI: 10.1080/00986445.2019.1573168

[20] Nguyen, T.H., Vu, A.-T. (2022). Preparation of B/ZnO Nanocomposite by Simple Mechanical Combustion Method for Removal of Antibiotics in Aqueous Environments. *Bulletin of Chemical Reaction Engineering & Catalysis*, 17 (4), 786-797. DOI: 10.9767/bcrec.17.4.16090.786-797

[21] Nguyen, T.H., Cong, T.A.N., Vu, A.-T. (2023). Synthesis of Carnation-Like ZnO for Photocatalytic Degradation of Antibiotics, Including Tetracycline Hydrochloride. *Environmental Engineering Science*. 40(8), 329-339. DOI: 10.1089/ees.2023.0034

[22] Nguyen, T.H., Vu, A.-T. (2023). Investigation of enhanced degradation of the antibiotic under visible in novel B/ZnO/TiO2 nanocomposite and its electrical energy consumption. *Nanotechnology,* 35(1), 015709. DOI: 10.1088/1361-6528/acffce

[23] Kim, M.G., Kang, J.M., Lee, J.E., Kim, K.S., Kim, K.H., Cho, M., Lee, S.G. (2021). Effects of calcination temperature on the phase composition, photocatalytic degradation, and virucidal activities of TiO2 nanoparticles. *ACS Omega*, 6(16), 10668-10678. DOI: 10.1021/acsomega.1c00043

[24] Lal, M., Sharma, P., Ram, C. (2021). Calcination temperature effect on titanium oxide (TiO2) nanoparticles synthesis. *Optik*, 241, 166934. DOI: 10.1016/j.ijleo.2021.166934

[25] Zhang, Z., Wang, C.-C., Zakaria, R., Ying, J.Y. (1998). Role of particle size in nanocrystalline TiO2-based photocatalysts. *The Journal of Physical Chemistry B*, 102(52), 10871-10878. DOI: 10.1021/jp982948+

[26] Hassani, A., Faraji, M., Eghbali, P. (2020). Facile fabrication of mpg-C3N4/Ag/ZnO nanowires/Zn photocatalyst plates for photodegradation of dye pollutant. *Journal of Photochemistry Photobiology A: Chemistry*, 400, 112665. DOI: 10.1016/j.jphotochem.2020.112665

[27] Arab Chamjangali, M., Bagherian, G., Bahramian, B., Fahimi Rad, B. (2015). Synthesis and application of multiple rods gold–zinc oxide nanostructures in the photocatalytic degradation of methyl orange. *International Journal of Environmental Science Technology*, 12, 151-160. DOI: 10.1007/s13762-014-0669-x

[28] Nasrollahzadeh, M.S., Hadavifar, M., Ghasemi, S.S., Arab Chamjangali, M. (2018). Synthesis of ZnO nanostructure using activated carbon for photocatalytic degradation of methyl orange from aqueous solutions. *Applied Water Science*, 8, 1-12. DOI: 10.1007/s13201-018-0750-6

[29] Nguyen, C.H., Fu, C.-C., Juang, R.-S. (2018). Degradation of methylene blue and methyl orange by palladium-doped TiO2 photocatalysis for water reuse: Efficiency and degradation pathways. *Journal of Cleaner Production*, 202, 413-427. DOI: 10.1016/j.jclepro.2018.08.110

[30] Nguyen, V.N., Tran, D.T., Nguyen, M.T., Le, T.T.T., Ha, M.N., Nguyen, M.V., Pham, T.D. (2018). Enhanced photocatalytic degradation of methyl orange using ZnO/graphene oxide nanocomposites. *Research on Chemical Intermediates*, 44, 3081-3095. DOI: 10.1007/s11164-018-3294-3

[31] Nguyen, L.T., Nguyen, L.T., Duong, A.T., Nguyen, B.D., Quang Hai, N., Chu, V.H., Nguyen, T.D., Bach, L.G. (2019). Preparation, characterization and photocatalytic activity of La-doped zinc oxide nanoparticles. *Materials*, 12(8), 1195. DOI: 10.3390/ma12081195

[32] Zhang, L., Qin, M., Yu, Y., Zhang, M., Zhao, X., Qian, J., Wu, H. (2019). Preparation of ternary Pt–NiO–ZnO hybrids and investigation of its photocatalytic performance toward methyl orange. *Journal of Materials Science: Materials in Electronics*, 30, 5158-5169. DOI: 10.1007/s10854-019-00814-2

[33] Janani, F., Khiar, H., Taoufik, N., Elhalil, A., Sadiq, M., Puga, A., Mansouri, S., Barka, N. (2021). ZnO–Al2O3–CeO2–Ce2O3 mixed metal oxides as a promising photocatalyst for methyl orange photocatalytic degradation. *Materials Today Chemistry*, 21, 100495. DOI: 10.1016/j.mtchem.2021.100495.